Available online at www.sciencedirect.com
SCIENCE DIRECT®
Journal of Computational Physics 207 (2005) 114–128
JOURNAL OF COMPUTATIONAL PHYSICS
www.elsevier.com/locate/jcp

A new method to impose no-slip boundary conditions in dissipative particle dynamics

Igor V. Pivkin *, George Em Karniadakis

Division of Applied Mathematics, Brown University, 182 George St., Box F, Providence, RI 02912, USA

Received 3 November 2004; received in revised form 3 January 2005; accepted 10 January 2005
Available online 12 February 2005

Abstract

Dissipative particle dynamics (DPD) is a potentially very effective approach in simulating mesoscale hydrodynamics. However, because of the soft potentials employed, the simple no-slip boundary conditions are difficult to impose. In this work, we first identify some of these difficulties and subsequently we propose a new method, based on an equivalent force between wall- and DPD-particles, to impose boundary conditions. We demonstrate the validity of this approach for steady problems (Poiseuille flow, lid-driven cavity) as well as for the unsteady oscillating flow over a flat plate.

Keywords: DPD; Boundary conditions; No-slip; Slip; Atomistic; Stochastic MD

1. Introduction

The dissipative particle dynamics (DPD) model consists of particles which correspond to *coarse-grained* entities, thus, representing molecular clusters rather than individual atoms. The particles move off-lattice interacting with each other through a set of prescribed and velocity-dependent forces [1,2]. Specifically, for simple fluids there are three types of forces acting on each dissipative particle:

- A purely repulsive conservative force.
- A dissipative force that reduces velocity differences between the particles.
- A stochastic force directed along the line connecting the center of the particles.

* Corresponding author. Tel.: +1 401 863 1217; fax: +1 401 863 3369.
E-mail addresses: piv@dam.brown.edu (I.V. Pivkin), gk@dam.brown.edu (G.E. Karniadakis).

0021-9991/$ - see front matter
doi:10.1016/j.jcp.2005.01.006

Let us consider a system consisted of N particles having equal mass (for simplicity in the presentation) m, position $\mathbf{r}_i$, and velocities $\boldsymbol{v}_i$. The aforementioned three types of forces exerted on a particle i by particle j are given by:

$$\mathbf{F}_{ij}^{\mathrm{C}} = \mathscr{F}_{ij}^{\mathrm{C}}(r_{ij})\hat{\mathbf{r}}_{ij}, \tag{1}$$

$$\mathbf{F}_{ij}^{\mathrm{D}} = -\gamma\omega^{\mathrm{D}}(r_{ij})(\boldsymbol{v}_{ij}\cdot\hat{\mathbf{r}}_{ij})\hat{\mathbf{r}}_{ij}, \tag{2}$$

$$\mathbf{F}_{ij}^{\mathrm{R}} = \sigma\omega^{\mathrm{R}}(r_{ij})\xi_{ij}\hat{\mathbf{r}}_{ij}, \tag{3}$$

where $\mathbf{r}_{ij}\equiv\mathbf{r}_i-\mathbf{r}_j$, $r_{ij}\equiv|\mathbf{r}_{ij}|$, $\hat{\mathbf{r}}_{ij}\equiv\mathbf{r}_{ij}/r_{ij}$, and $\boldsymbol{v}_{ij}\equiv\mathbf{v}_i-\mathbf{v}_j$. The variables γ and σ determine the strength of the dissipative and random forces, respectively. Also, ξ_{ij} are symmetric Gaussian random variables with zero mean and unit variance, and are independent for different pairs of particles and at different times; $\xi_{ij}=\xi_{ji}$ is enforced in order to satisfy momentum conservation. Finally, ω^{D} and ω^{R} are weight functions.

All forces are acting within a sphere of *interaction radius* r_{c}, which is the length scale of the system. The conservative force is given by a soft potential (see [3]):

$$\mathbf{F}_{ij}^{\mathrm{C}} = \begin{cases} a_{ij}(1-r_{ij}/r_{\mathrm{c}})\hat{\mathbf{r}}_{ij} & \text{for } r_{ij}\leqslant r_{\mathrm{c}}=1,\\ 0 & \text{for } r_{ij}>r_{\mathrm{c}}=1, \end{cases}$$

$a_{ij}=\sqrt{a_i a_j}$, where a_i and a_j are conservative force coefficients for particle i and particle j. The requirement of canonical distribution sets two conditions on the weight functions and the amplitudes of the dissipative and random forces, see [2]. Specifically, we have that:

$$\omega^{\mathrm{D}}(r_{ij}) = \left[\omega^{\mathrm{R}}(r_{ij})\right]^2 \tag{4}$$

and

$$\sigma^2 = 2\gamma k_{\mathrm{B}}T, \tag{5}$$

where T is the system temperature and k_{B} the Boltzmann constant. The weight function takes the form:

$$\omega^{\mathrm{R}}(r_{ij}) = \begin{cases} 1-r_{ij}/r_{\mathrm{c}} & \text{for } r_{ij}\leqslant r_{\mathrm{c}},\\ 0 & \text{for } r_{ij}>r_{\mathrm{c}}. \end{cases}$$

The time evolution of DPD particles is described by Newton's law:

$$\mathrm{d}\mathbf{r}_i = \boldsymbol{v}_i\mathrm{d}t, \tag{6}$$

$$\mathrm{d}\boldsymbol{v}_i = \frac{1}{m}\left(\mathbf{F}_i^{\mathrm{C}}\mathrm{d}t + \mathbf{F}_i^{\mathrm{D}}\mathrm{d}t + \mathbf{F}_i^{\mathrm{R}}\sqrt{\mathrm{d}t}\right). \tag{7}$$

Here, $\mathbf{F}_i^{\mathrm{C}}=\sum_{i\neq j}\mathbf{F}_{ij}^{\mathrm{C}}$ is the total conservative force acting on particle i; $\mathbf{F}_i^{\mathrm{D}}$ and $\mathbf{F}_i^{\mathrm{R}}$ are defined similarly.

There are several methods in integrating the DPD evolution equations; for a comparison of different integrators see [4], and for a new and potentially more robust time integrator see [5]. While high-order accurate solution methods are still under investigation, the main issue for DPD simulations in confined geometries is the imposition of boundary conditions, specifically at solid boundaries. To this end, the boundary conditions that have been used in DPD are based on general ideas implemented both in lattice Boltzmann method (LBM) and molecular dynamics (MD) formulations. However, unlike the MD method, the soft repulsion between DPD particles cannot prevent fluid particles from penetrating solid boundaries, and thus extra effort is required to impose accurately the no-slip (or partial slip) wall boundary condition. To the best of our knowledge, although good progress has been made, there is no yet consensus as to what

type of boundary conditions performs best, especially in the presence of conservative forces as well as in complex-geometry flows.

A broad classification of the three main approaches to impose boundary conditions in DPD was provided in [6] as follows:

1. The Lees–Edwards method to impose planar shear, also used in LBM [7], which is essentially a way to avoid modeling directly the physical boundary [8–10].
2. Freezing regions of the fluid to create a rigid wall or a rigid body, e.g. in particulate flows, see [1,9].
3. Combine different types of particle-layers with proper reflections, namely specular reflection, bounce-back reflection, or Maxwellian reflection [11–13].

We will use the Lees–Edwards method later in Section 3.2, so here we provide its brief description. Consider a system of particles in a periodic box and assume that the upper wall is moving with velocity $U_x/2$ and lower wall with $-U_x/2$. Lees and Edwards [8] suggested a method to simulate such shear flow by applying modified periodic boundary conditions. A particle crossing the upper boundary of the box at time t is re-introduced through the lower boundary with its x-coordinate shifted by $-U_x t$ and the x-velocity decreased by U_x. For a particle crossing the lower boundary of the box the x-coordinate shift is $U_x t$ and the x-velocity is increased by U_x. In addition, in computing the force between particle i interacting with particle j through the upper (lower) boundary, $-U_x$ ($+U_x$) should be added to the relative velocity $\boldsymbol{v}_{ij}$.

The third category is indeed quite broad, and the technical details in the various implementations published so far are quite different. Since the method proposed in this paper also employs particle-layers as well as reflections, we review in some more detail the most representative works published so far that fall under category (3).

In Revenga et al. [11], a particle-layer is stuck on the solid boundary and effective dissipative and random forces are obtained analytically on the DPD fluid particles by assuming a continuum limit. However, reflections were found necessary to reflect particles back into the fluid when they cross the wall since the effective computed forces are not sufficient to prevent wall penetration. In Revenga et al. [6], the effect of specular, Maxwellian and bounce-back reflections was also investigated. In specular reflections the velocity component tangential to the wall does not change while the normal component is reversed. In the bounce-back reflection both components are reversed. A Maxwellian reflection involves particles that are introduced back into the flow with a velocity following a Maxwellian distribution centered around the wall velocity. In Revenga et al. [6], a key non-dimensional parameter was identified that affects the wall slip velocity. Specifically, there are five governing parameters in the DPD fluid system: m (the mass of particles); γ (the friction coefficient); r_c (the cut-off radius); $k_B T$ (temperature); and $\lambda_d = n^{-1/d}$ (the average distance between particles, where d is the space dimension and n is the number density). We can define the dimensionless friction coefficient

$$\tau \equiv \frac{\gamma \lambda}{d v_T},$$

where $v_T = \sqrt{k_B T/m}$ is the thermal velocity. Large values of τ mean that the particles move very little in the time scale associated with the velocity decaying due to thermal fluctuations. In Revenga et al. [6], the plane Couette flow was considered in order to evaluate the above boundary conditions. The Lees–Edwards boundary conditions work well for this model but the objective is to see what type of reflections are appropriate with their particle-layer approach. It was shown in [6] that for large values of τ all three reflections satisfy the no-slip condition. However, for small values of τ the specular and Maxwellian reflections produce an excessive slip velocity at the wall while the bounce-back approach satisfies the no-slip condition. An anomaly, however, was observed for the temperature profile very close to the wall at small values of τ even with the bounce-back boundary conditions. Another problem with the approach of Revenga et al. [6] is that

the computation of forces is analytical and thus it cannot be easily extended to non-planar walls. In addition, the more difficult case where conservative forces are present was not considered. As we shall see below, this is an important case as it induces large density fluctuations at the wall.

In Willemsen et al. [12], an extra particle-layer is included on the outside of the domain with the objective of constructing a correct velocity profile that continues *beyond* the wall boundary. The position and velocities of particles inside that layer are determined from a layer of DPD particles adjacent to the boundary and within distance r_c (the interaction radius). For example, to impose zero velocity at a solid boundary, points in the particle-layer outside the domain have tangential and normal velocity components opposite from the original. When a DPD particle hits the boundary, then a bounce-back reflection is imposed. This approach works very well in the absence of conservative forces but when conservative forces are present density oscillations occur. In this case, a second layer of DPD particles was introduced by Willemsen et al. [12] between r_c and $2r_c$ in order to compute the repulsive interaction. This approach seems to reduce but not totally eliminate the density fluctuations at the walls. Overall, the method of Willemsen et al. [12] is quite effective but it may not be easily implemented in complex-geometry flows, e.g. flow around a cube, as it is not clear how to construct such "ghost" particle-layers in such situations.

Finally, in the third category above we have also included another implementation reported in [13]. In this implementation, frozen particles are used to represent the wall but there is an extra thin layer of DPD particles inside the domain and adjacent to the solid boundary where the no-slip boundary condition holds. Specifically, a random velocity distribution with zero mean is enforced in this layer with corresponding particle velocity

$$\boldsymbol{v}_i = \boldsymbol{v}_R + \mathbf{n}\left(\sqrt{(\mathbf{n}\cdot\boldsymbol{v}_R)^2} - \mathbf{n}\cdot\boldsymbol{v}_R\right),$$

where $\boldsymbol{v}_R$ is the random vector and $\mathbf{n}$ is the unit vector towards the flow domain. The thickness of the layer in channel flows is selected as the minimum between 0.5% of the channel width and $r_c/2$; this thin layer is necessary to prevent the frozen wall to cool down the DPD fluid. Nevertheless, some temperature drop at the wall boundaries is present in the simulation results reported in [13], which is undesirable.

The objective of the current work is to produce a systematic way of imposing the no-slip boundary condition. The method we propose is under the general category (3) of the aforementioned list and can be easily implemented for simple- and complex-geometry flows. The main idea is to provide a systematic procedure to compute the repulsion force exerted by the wall particles on the fluid in combination with bounce-back reflections, across a wide range of densities for liquids. The new method is verified for Poiseuille flow, Stokes flow over an oscillating plate, and for the lid-driven cavity, using both analytical solutions and corresponding high-order accurate Navier–Stokes solutions.

2. Diagnostic DPD simulations

In order to appreciate the degree of difficulty in imposing no-slip boundary conditions with the DPD method as well as to identify the most influential parameters, we first perform some diagnostic DPD simulations for Poiseuille flow in a channel. The flow domain is a cube with size 10, and periodic boundary conditions are imposed along two directions, see Fig. 1. In order to sustain the flow an external body force equal to 0.02 (DPD units) is imposed. The density of the DPD fluid is $n_f = 3$ and the temperature is $k_B T = 1$. The random and dissipative forces are defined by the parameters $\sigma = 3$ and $\gamma = 4.5$, respectively, while the conservative force parameter is set to $a_f = 25$. We simulate the solid walls by freezing the DPD particles in the wall regions. The wall particles interact with fluid particles, however, we do not allow them to move. In some cases we will also use bounce-back boundary conditions. In order to investigate the effect of the wall density, we will use different values for the number density of the walls, n_w. In addition, we will vary the

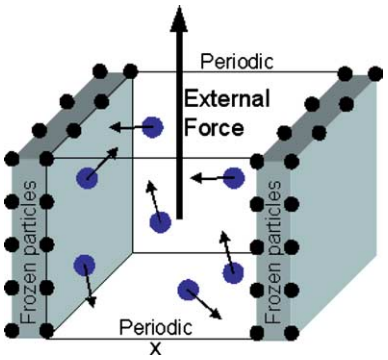

Fig. 1. Sketch of the cubic domain for simulating Poiseuille flow. Periodic boundary conditions are imposed in two directions. The walls are simulated by freezing DPD particles.

conservative (also called repulsive) force coefficient for the wall particles, a_w. The results we will present below are obtained by subdividing the domain into 100 bins across the channel, while the simulations were run for 200,000 time steps and the results were averaged over the last 40,000 time steps.

First, we simulate the case with the walls modeled by freezing the DPD particles in two layers inside each wall region. The walls have the same density as the fluid, i.e., $n_w = n_f$, and the conservative force of the wall DPD particles, a_w, is the same as of the fluid particles, a_f. The results of the simulations are shown in Fig. 2. The dashed line is density, the dash-dotted line is partial temperature along the periodic cross-flow direction and triangles is the velocity profile across the channel. The dotted lines are the Navier–Stokes solutions corresponding to no-slip boundary conditions. The main finding here is that the fluid particles can penetrate wall regions, as it can be seen from the non-zero density of the fluid particles inside the walls. This is the result of the soft repulsive forces employed in the DPD formulation. In order to prevent the fluid particle

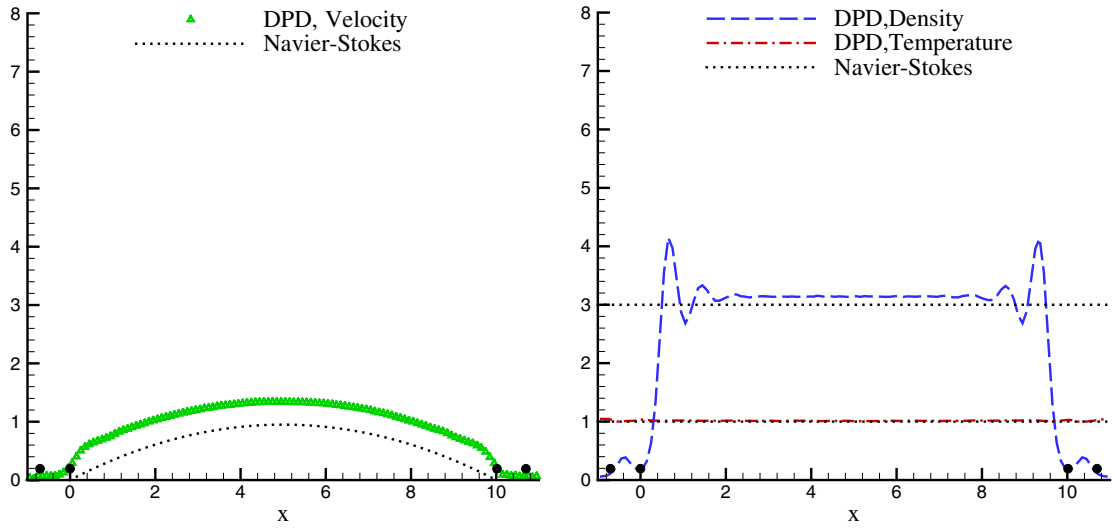

Fig. 2. Left: Velocity profile. Right: Density and temperature profiles. The walls are simulated by freezing DPD particles ($n_w = n_f$; $a_w = a_f$).

from penetrating the walls we can increase the wall density or the repulsion (conservative) force of the wall particles.

Next, we increase the wall density to be four times higher than fluid density. The results from these DPD simulations are shown in Fig. 3. There is no fluid penetration into the wall regions, however, large density fluctuations appear across the channel. The density level of the fluid in the middle of the channel is elevated and there are almost no particles close to the walls. The fluid is squeezed towards the middle of the channel by the wall particles leading to a large velocity slip.

If we increase the repulsion force of the wall particles, keeping the wall density the same as fluid density, we obtain similar results as before as shown in Fig. 4. Again, density fluctuations and large slip are observed. From these results we conclude, that to prevent fluid particles from penetrating the walls increasing the wall density of wall particles or the repulsion force may not be an effective solution.

We now return to the first test case above and employ the bounce-back boundary condition on the surface of the walls, keeping the density and the conservative force of the wall particles the same as of fluid particles. From the results shown in Fig. 5, we can see that the fluid density is low close to the wall. This is due to the excessive repulsion of fluid particles away from the walls. One way to fix this problem is to shift the wall particles away from the fluid–solid interface. The question is how to choose the shift distance? A straightforward approach is to shift the wall particles by half inter-particle distance, which is $\frac{1}{2}n_{\mathrm{f}}^{-1/3}$. The results from such simulations are shown in Fig. 6. The density fluctuations are less pronounced than in previous cases while the level of the density in the middle of the channel is close to the desired level. The velocity profile has improved, although some slip is still present. When we fix the density profile by shifting wall particles, we also reduce the dissipative force (or friction) between the fluid particles and the walls; the latter depends on the distance between particles. Bounce-back boundary conditions compensate this effect, however, this correction may not always be sufficient and may lead to some small slip, as we can see from the results of Fig. 6.

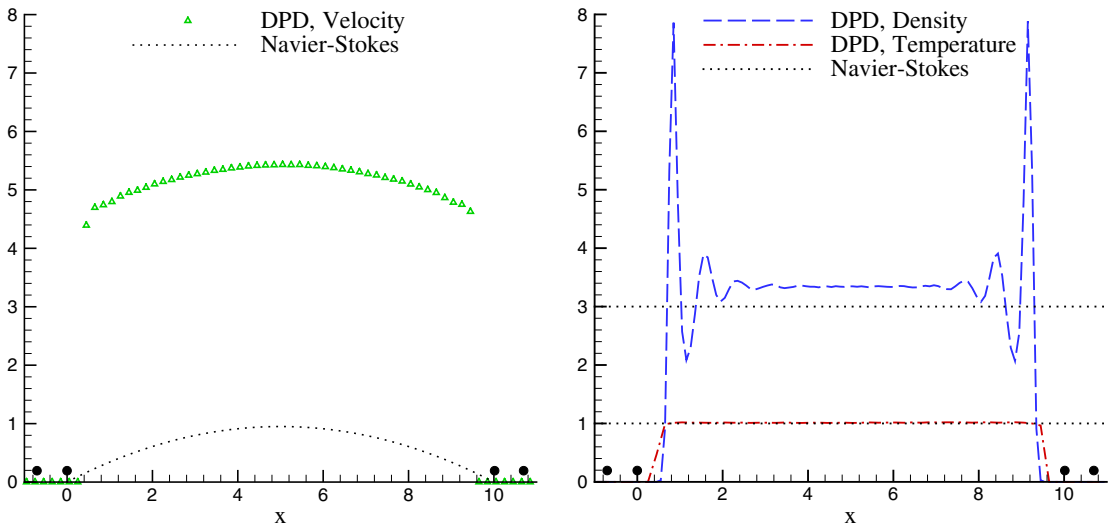

Fig. 3. Left: Velocity profile. Right: Density and temperature profiles. ($n_{\mathrm{w}} = 4n_{\mathrm{f}}$; $a_{\mathrm{w}} = a_{\mathrm{f}}$). The walls are simulated by freezing DPD particles.

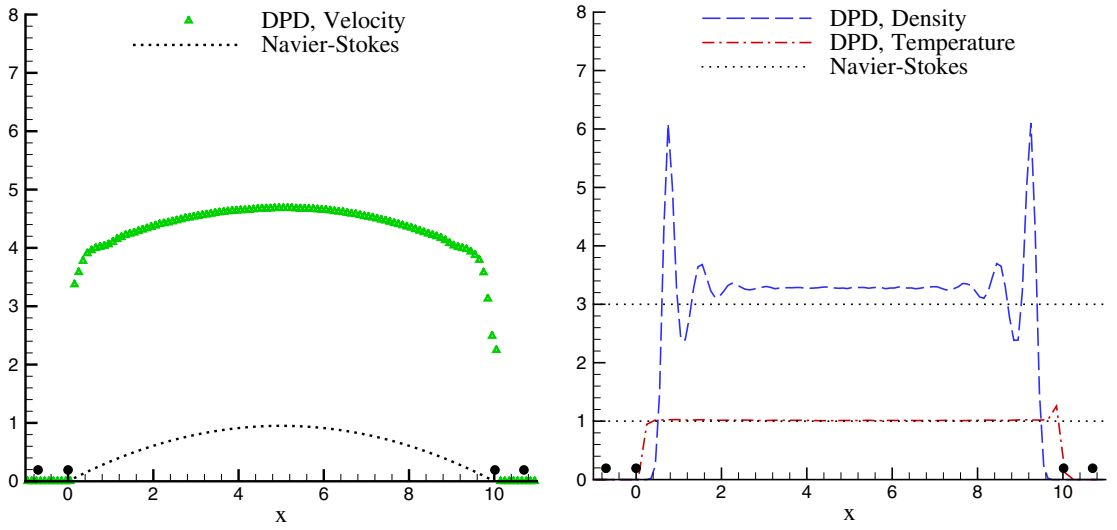

Fig. 4. Left: Velocity profile. Right: Density and temperature profiles. ($n_w = n_f$; $a_w = 4a_f$). The walls are simulated by freezing DPD particles.

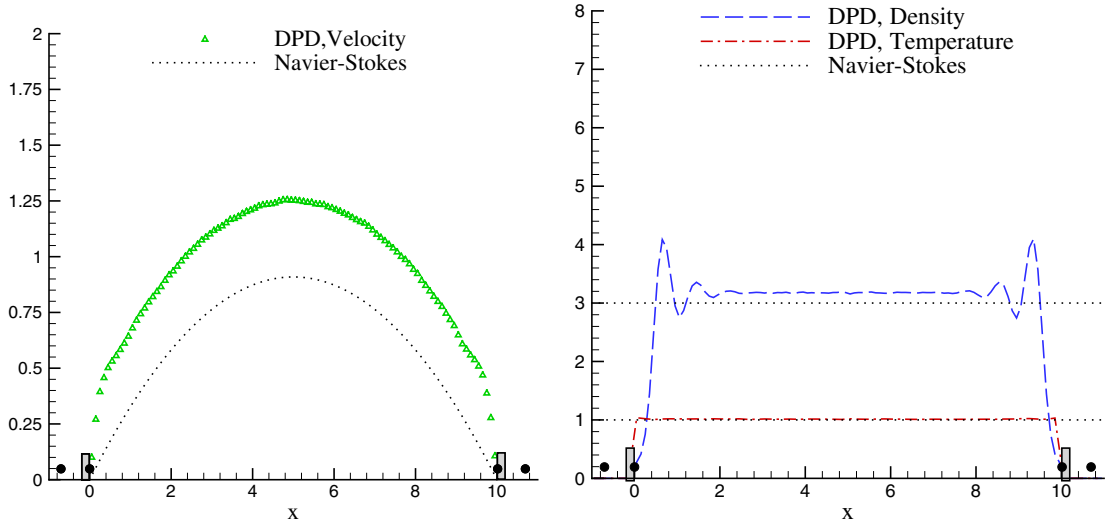

Fig. 5. Left: Velocity profile. Right: Density and temperature profiles. ($n_w = n_f$; $a_w = a_f$). The walls are simulated by freezing DPD particles in combination with bounce-back boundary conditions (shown as shaded rectangles).

3. New boundary conditions

In this section, we propose a new procedure to apply no-slip boundary conditions building on what we presented in the previous section. Let us consider the wall, which is created by freezing layers of DPD particles, see Fig. 7. The particles are distributed on a regular lattice with distance $n_w^{-1/3}$. We know the structure of the wall and the conservative force, so we can calculate the force exerted by the wall particles.

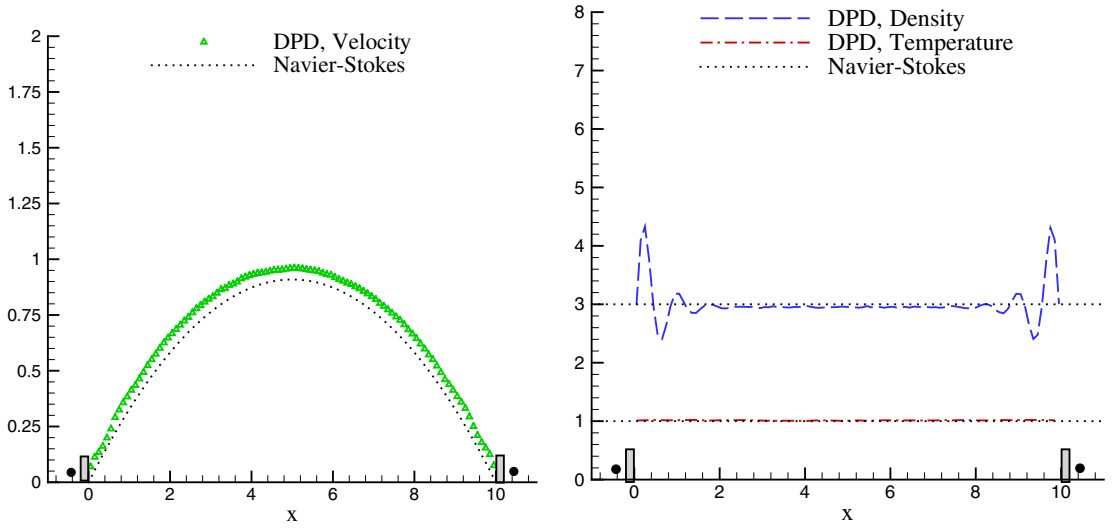

Fig. 6. Left: Velocity profile. Right: Density and temperature profiles. ($n_w = n_f$; $a_w = a_f$). The walls are simulated by freezing DPD particles in combination with bounce-back boundary conditions. The wall particles are shifted by half inter-particle distance.

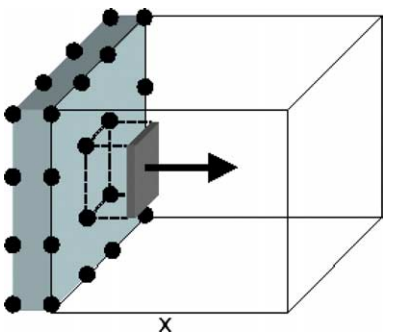

Fig. 7. Sketch of an imaginary plane on which we compute the force exerted by the wall particles.

Specifically, to compute the average force per unit area due to wall particles we used $30 \times 30 = 900$ points. They were uniformly distributed over a square patch with size $n_w^{-1/3}$ that was placed within a specified distance from the wall. The average force was taken to be the arithmetic average over force at these 900 points. The plot of this force per unit area against the distance from the wall is shown in Fig. 8.

We note here that this force is proportional to the effective wall–fluid particle conservative force parameter, $a_e = \sqrt{a_w a_f}$. Next, we compute the total force per unit area exerted by the wall particles for *different* values of the wall density; the total force is the area under the curve in Fig. 8. Subsequently, we fit a second-order polynomial using the computed values to obtain an analytic approximation for the total force in the range of densities from $n_w = 3$ to 25, and the results are shown in Fig. 9. We have set the coefficient a_e to 1.0 in these computations. The approximation we obtained for the total force is

$$F_w = a_e(0.0303n_w^2 + 0.5617n_w - 0.8536), \tag{8}$$

where n_w is the wall density. This approximation is valid only for wall density n_w variations between 3 and 25. For other values of the wall density or different wall structure (e.g. FCC lattice) we can employ a similar procedure to obtain the total force F_w.

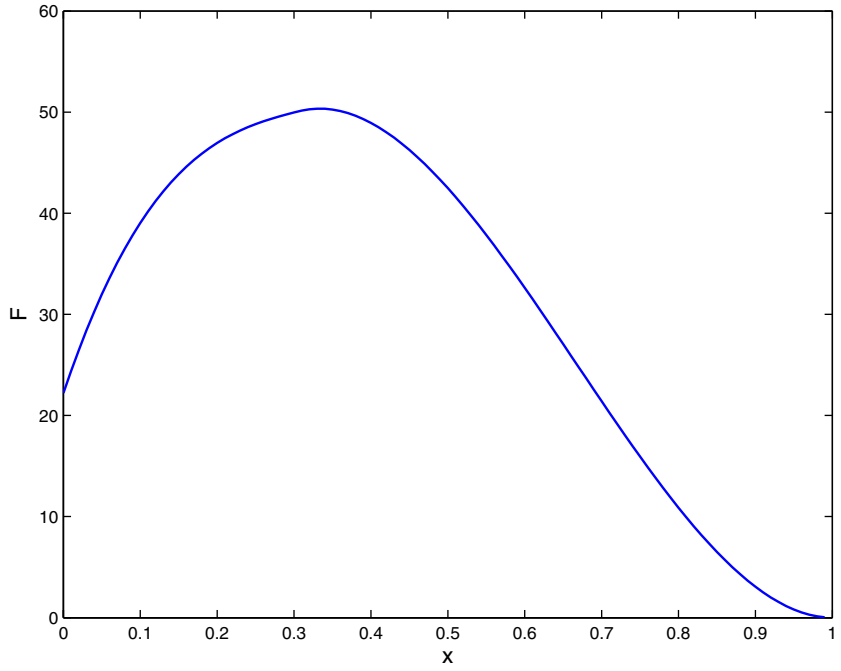

Fig. 8. Force exerted by wall particles per unit area against the distance from the wall.

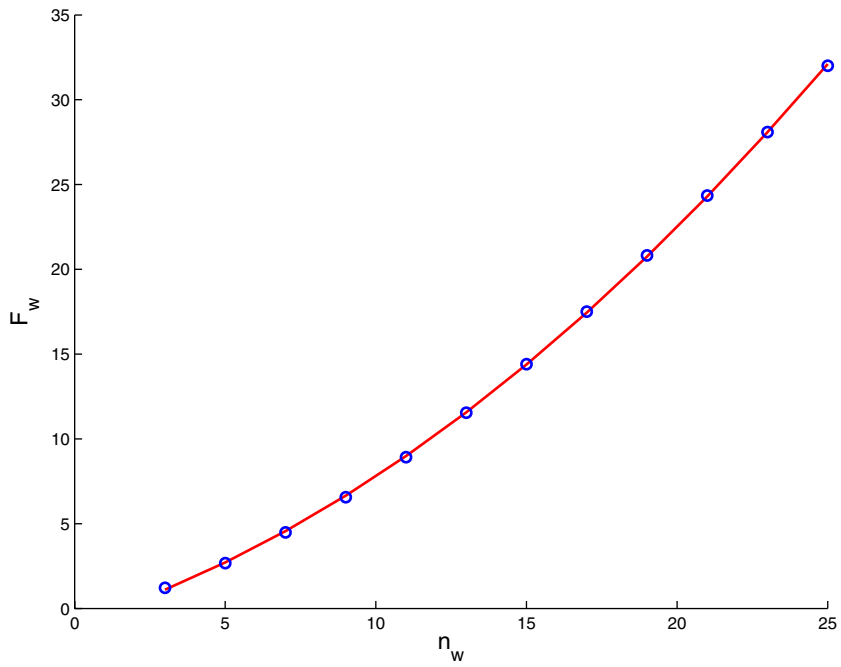

Fig. 9. Computed total force from the wall – circles; second-order polynomial fit – solid line. The effective repulsive force coefficient a_e is set to 1.0 here.

We now consider the fluid in the cubic domain and ignore for the moment the presence of the walls. If we place an imaginary plane on the surface of the simulation domain the force exerted by fluid per unit area in this plane will be equal to the pressure of the fluid, which can be estimated by the expression, see [3]

$$P = n_f k_B T + 0.1 a_f n_f^2. \tag{9}$$

If we move this imaginary plane away from the wall, the force decreases and at one cut-off distance r_c from the wall it is zero. Our objective now is to adjust the wall particle repulsion force coefficient, a_w – and as a result the effective conservative force coefficient, a_e – in such way, that if we place a particle within one cut-off distance from the wall, the average force acting from the wall will be equal to the force from the fluid. We can parameterize the total force per unit area from the fluid as αP. A value of α that gives good results in simulations for DPD fluid densities considered in this paper is 0.39. Specifically, for $\alpha = 0.39$, the computed fluid density level in the middle of the channel is within 1% from desired value. For fluid densities not considered in this paper, α may be adjusted appropriately.

In summary, the final result is that we can estimate the value of the conservative force coefficient of wall particles from

$$a_w = \frac{a_e^2}{a_f}, \tag{10}$$

where

$$a_e = \frac{0.39(n_f k_B T + 0.1 a_f n_f^2)}{(0.0303 n_w^2 + 0.5617 n_w - 0.8536)}. \tag{11}$$

In the following, we will present several prototype flow examples in order to evaluate the proposed boundary conditions.

3.1. Poiseuille flow

The first test case is Poiseuille flow, as in the previous section, with the density of the fluid and the wall density equal to 3. We use bounce-back boundary conditions on the surface of the wall. The conservative force of the wall particles is adjusted as described above, see Eq. (10), and it is equal to $a_w = 3.2447$. As we

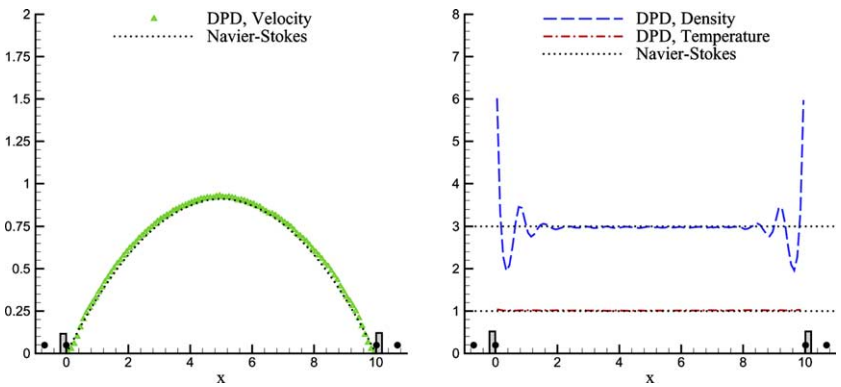

Fig. 10. Left: Velocity profile. Right: Density and temperature profiles. The walls are simulated by freezing DPD particles in combination with bounce-back boundary conditions. The conservative force of the wall particles is computed as described in the text. ($n_w = n_f = 3$; $a_w = 3.2447$).

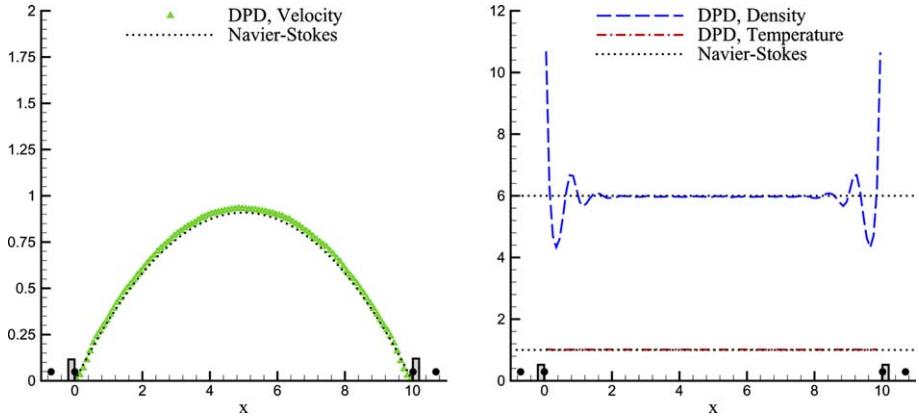

Fig. 11. Poiseuille flow. Left: Velocity profile. Right: Density and temperature profiles. The walls are simulated by freezing DPD particles in combination with bounce-back boundary conditions. The conservative force of the wall particles is computed as described in the text. ($n_w = n_f = 6$; $a_w = 2.4320$).

can see in Fig. 10, we have some residual density variations at the ends of the channel, however in the middle of the channel the density has the desired level. In addition, we satisfy the no-slip conditions. Similar cases for density equal to 6 and 9 are shown in Figs. 11 and 12, where the wall particle conservative force coefficients are equal to 2.4320 and 2.4111, respectively.

We have also verified the DPD code by repeating case A (Poiseuille flow of simple DPD fluid) considered in [13]. The simulation parameters are the same as in the original paper except the implementation of no-slip boundary conditions. We use two layers of freezed DPD particles inside each wall region, in combination with bounce-back reflection. The conservative force coefficient for wall particles is computed as described above and is equal to 2.6588. The results of simulations are in a very good agreement with [13]. In particular, the computed fluid velocity in the middle of the channel is 8.633 in comparison to the value 8.639 predicted in [13].

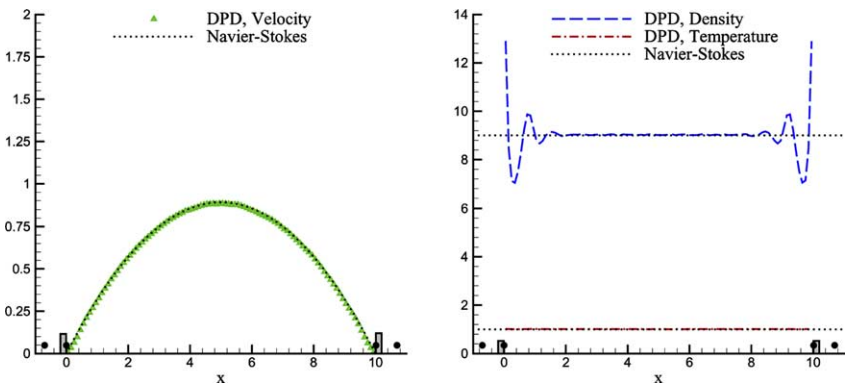

Fig. 12. Poiseuille flow. Left: Velocity profile. Right: Density and temperature profiles. The walls are simulated by freezing DPD particles in combination with bounce-back boundary conditions. The conservative force of the wall particles is computed as described in the text. ($n_w = n_f = 9$; $a_w = 2.4111$).

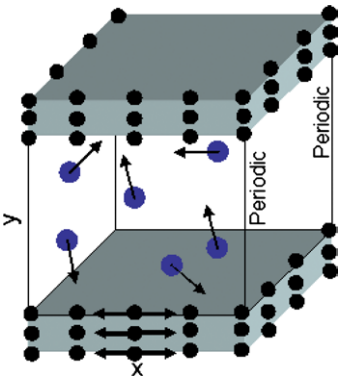

Fig. 13. Stokes oscillating plate problem. The fluid domain is a cube, periodic in two directions. The walls are simulated by freezing DPD particles, in combination with bounce-back boundary conditions. The lower wall is oscillating.

3.2. Unsteady Stokes flow

Next, we consider an unsteady case, namely Stokes flow over an oscillating flat plate, for which an analytic solution exists, see [14]. The fluid domain is a cube with size 10, while periodicity is imposed along two directions, see Fig. 13. The lower wall is oscillating with velocity $U_x = \sin(\Omega t)$, where $\Omega = \pi/20$. The density of the DPD fluid is $n_f = 10$, and the temperature is set to $k_B T = 1/3$. The random and dissipative force coefficients, σ and γ, are 1.73205 and 4.5, respectively. The conservative force coefficient of fluid particles, a_f, is set to 3. The dynamic viscosity of the fluid was determined from the plane Couette flow simulations with Lees–Edwards boundary conditions and is equal to 2.19. The walls are modeled as *three layers* of DPD particles which move with prescribed velocity U_x, in combination with bounce-back boundary conditions. Specifically the bounce-back rule is now implemented in a reference frame where the wall is stationary. The conservative force for wall particles is computed as described earlier, see Eq. (10); we obtained $a_w = 0.9275$. The domain was subdivided into 20 bins in the x- and y-directions, and data were collected at 16 points

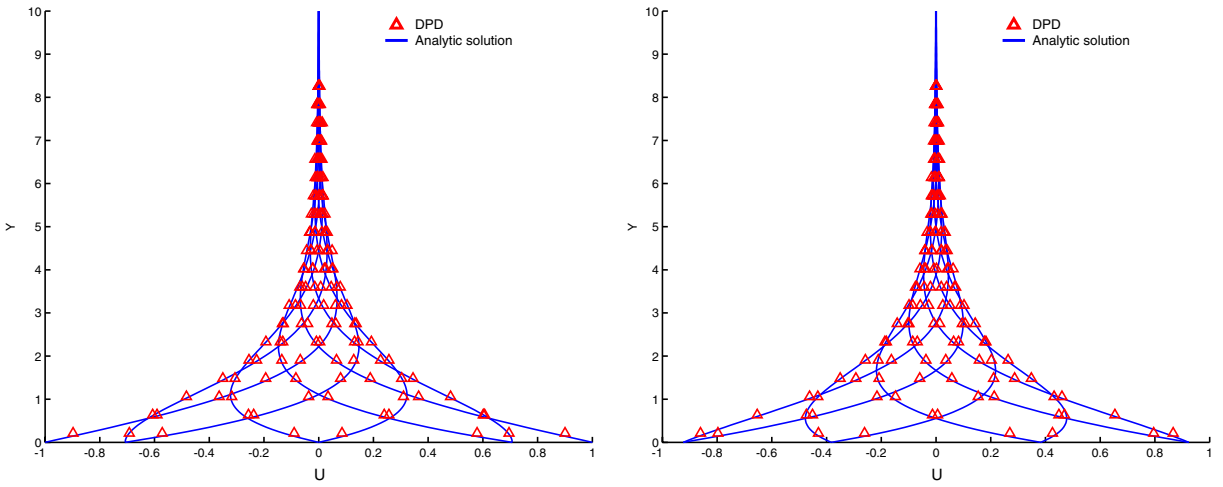

Fig. 14. Unsteady stokes flow. Shown are flow velocity profiles at 16 instances during the period. Left: Time $t = 2k\pi/8$, $k = 0,\ldots,7$. Right: $t = (2k + 1)\pi/8$, $k = 0,\ldots,7$. DPD simulations – triangles; exact solution – line.

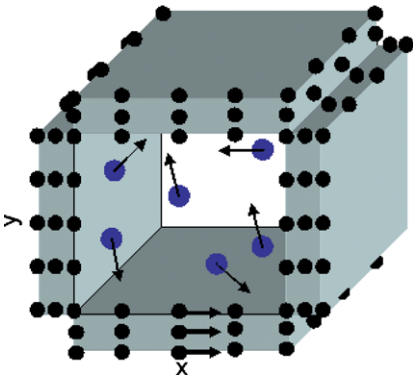

Fig. 15. Lid-driven cavity flow. The fluid domain is a cube, periodic in one direction. The walls are simulated by freezing DPD particles in combination with bounce-back boundary conditions. The lower wall is moving with constant velocity.

during the periodic cycle by phase-averaging over the last 5 time steps over 50 periods. The fluid velocity profiles at 16 instances during one full period plotted against the normalized distance from the oscillating wall are shown in Fig. 14. The normalized distance is defined as $Y = y(\nu/\Omega)^{-1/2}$, where ν is kinematic viscosity of the fluid. The analytic solution is shown with solid line, while the DPD results are shown with triangles. The results of DPD simulations are in a good agreement with the analytic solution. We note here that the results are very sensitive to the boundary conditions. In the presence of slip at the oscillating wall, the lower points on the sides of the plot will not match the analytic solution.

3.3. Finite Reynolds number lid-driven cavity flow

Next, we consider flow in a lid-driven cavity at finite values of Reynolds number and we compare results with high-order accurate Navier–Stokes solutions. The DPD simulation parameters are similar to the previously described case. Here, the lower wall is moving with a constant velocity, $U_x = 0.5475$, see Fig. 15,

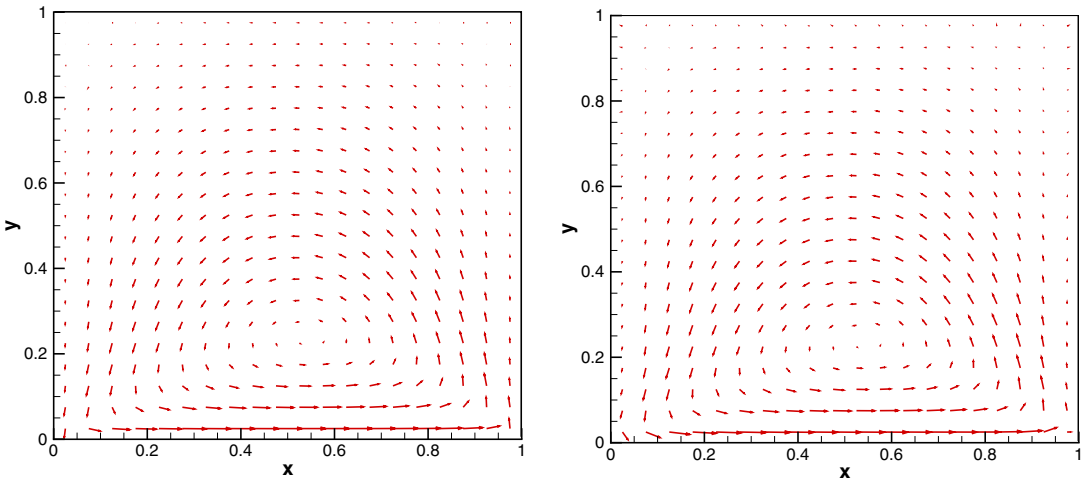

Fig. 16. Lid-driven cavity flow. Velocity vector field comparison. On the left, results from spectral element simulations; on the right, results from DPD simulations. The coordinates are normalized by the domain size, velocity by U_x.

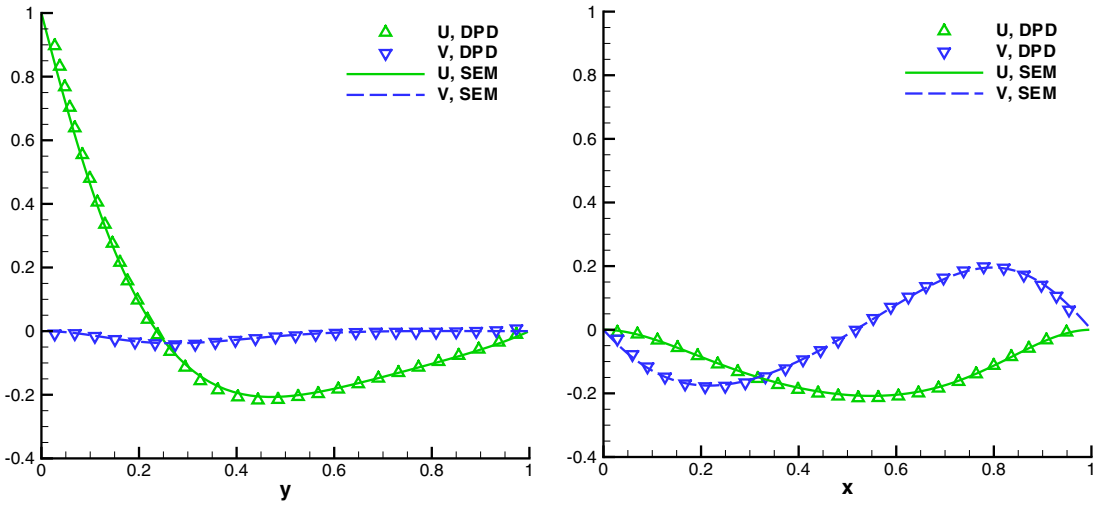

Fig. 17. Lid-driven cavity flow. Velocity profiles extracted along the vertical and horizontal lines. The coordinates are normalized by the domain size, velocity by U_x.

and the Reynolds number is 25. The simulation results are averaged over 200,000 time steps. We compare DPD results with spectral element simulation results based on the solver NEKTAR [15]. Specifically, the 2D spectral element simulations were performed in a square domain. The size of the domain is 1×1; it is discretized into 900 quadrilateral spectral elements with fourth-order polynomial expansion employed in each element. On one wall, a constant velocity is prescribed, $U_x = 1.0$ while no-slip boundary conditions are used on other walls. The Reynolds number is set to 25.

In Fig. 16, we present the computed velocity vector fields for spectral element and DPD simulations. We have good agreement between the two simulations. We extract two velocity profiles, vertical and horizontal cuts through the center of the domain, and present a more detailed comparison of simulation results in Fig. 17. On the left, the velocity magnitudes along the vertical cut and on the right along the horizontal cut are shown. The spectral element simulation results are shown with lines, DPD results are shown with triangles. Again, we have very good agreement.

4. Summary

In this paper we have introduced a new approach to impose the no-slip boundary condition for simple- and complex-geometry flows. The main result is summarized in Eqs. (10) and (11) that present formulas for the wall conservative parameter and the effective wall–fluid particle conservative parameter. The specific formulas given are for a fluid with density n_f in the range between 3 and 25, which covers values most often used in DPD simulations. For other densities a similar procedure, as the one we outlined here, can be developed to obtain an effective wall-particle interaction force. The presence of some density fluctuations in narrow regions very close to the boundaries is caused by the conservative forces but this does not seem to have an adverse effect on the velocity or the temperature distribution. To the best of our knowledge, all published methods for imposing no-slip condition exhibit some degree of density fluctuations, even the method of Willemsen et al. [12], where the velocity profile extends beyond the surface and into the wall solid boundary. In ongoing work, we have also verified the validity of the proposed method in flow around a periodic array of square cylinders against molecular dynamics simulations. A more systematic study for such more complex-geometry flows and also at higher Reynolds number will be presented in a future publication.

While we have established agreement between DPD and Navier–Stokes equations with no-slip wall surfaces, we have not yet explored the interesting area of the non-continuum effects, e.g. in sub-micron sized channels, where slip may be present [16]. Such study will require a new procedure to impose slip boundary conditions in DPD based on Maxwellian reflections instead of the bounce-back reflections which are more robust for imposing the no-slip boundary condition, see [6]. This issue, however, is not trivial and has not been fully resolved yet even for the lattice Boltzmann method (LBM), see discussions in [17,18], and in [19].

Acknowledgment

This work was supported by NSF (Grant No. CTS-0326720).

References

[1] P.J. Hoogerburgge, J.M. Koelman, Simulating microscopic hydrodynamic phenomena with dissipative particle dynamics, Europhys. Lett. 19 (3) (1992) 155–160.
[2] P. Espanol, P. Warren, Statistical mechanics of dissipative particle dynamics, Europhys. Lett. 30 (4) (1995) 191–196.
[3] R.D. Groot, P.B. Warren, Dissipative particle dynamics: bridging the gap between atomistic and mesoscopic simulation, J. Chem. Phys. 107 (11) (1997) 4423–4435.
[4] P. Nikunen, M. Karttunen, I. Vattulainen, How would you integrate the equations of motion in dissipative particle dynamic simulations? Comp. Phys. Commun. 153 (2003) 407–423.
[5] E. Peters, Elimination of time step effects in DPD, Europhys. Lett. 66 (3) (2004) 311–317.
[6] M. Revenga, I. Zuniga, P. Espanol, Boundary conditions in dissipative particle dynamics, Comp. Phys. Commun. 121–122 (1999) 309–311.
[7] A.J. Wagner, I. Pagonabarraga, Lees–Edwards boundary conditions for Lattice Boltzmann, J. Stat. Phys. 107 (2002) 521–537.
[8] A.W. Lees, S.F. Edwards, The computer study of transport processes under extreme conditions, J. Phys. C 5 (1972) 1921.
[9] E. Boek, P. Coveney, H. Lekkererker, P. van der Schoot, Simulating the rheology of dense colloidal suspensions using dissipative particle dynamics, Phys. Rev. E 55 (1997) 3124–3133.
[10] E. Boek, P. Coveney, H. Lekkererker, Computer simulation of rheological phenomena in dense colloidal suspensions with dissipative particle dynamics, J. Phys. Condens. Matter 8 (1996) 9509–9512.
[11] M. Revenga, I. Zuniga, P. Espanol, Boundary model in DPD, Int. J. Mod. Phys. C 9 (1998) 1319.
[12] S.M. Willemsen, H.C. Hoefsloot, P.D. Iedema, No-slip boundary condition in dissipative particle dynamics, Int. J. Mod. Phys. 11 (5) (2000) 881–890.
[13] X. Fan, N. Phan-Thien, N. Yong, X. Wu, D. Xu, Microchannel flow of a macromolecular suspension, Phys. Fluid 15 (1) (2003) 11–21.
[14] R. Panton, Incompressible Flow, Wiley, New York, 1996.
[15] G. Karniadakis, S. Sherwin, Spectral/hp Element Methods for CFD, Oxford University Press, New York, 1999.
[16] G. Karniadakis, A. Beskok, Microflows, Fundamentals and Simulation, Springer, New York, 2001.
[17] B. Li, D.Y. Kwok, Discrete Boltzmann equation for microfluidics, Phys. Rev. Lett. 90 (12) (2003) 124502.
[18] L.-S. Luo, Comment on "Discrete Boltzmann equation for microfluidics", Phys. Rev. Lett. 92 (13) (2004) 139401.
[19] S. Ansumali, I.V. Karlin, Kinetic boundary conditions in the lattice Boltzmann equation, Phys. Rev. E 66 (2002) 026311.